CHEMISTRY
A EUROPEAN JOURNAL

DOI: 10.1002/chem.201001852

Electronic and Optical Properties in the Solid-State Molecular Assemblies of Anion-Responsive Pyrrole-Based π-Conjugated Systems

Hiromitsu Maeda,*[a, b] Yuya Bando,[a] Yohei Haketa,[a] Yoshihito Honsho,[c] Shu Seki,*[b, c] Hiromi Nakajima,[d] and Norimitsu Tohnai*[d]

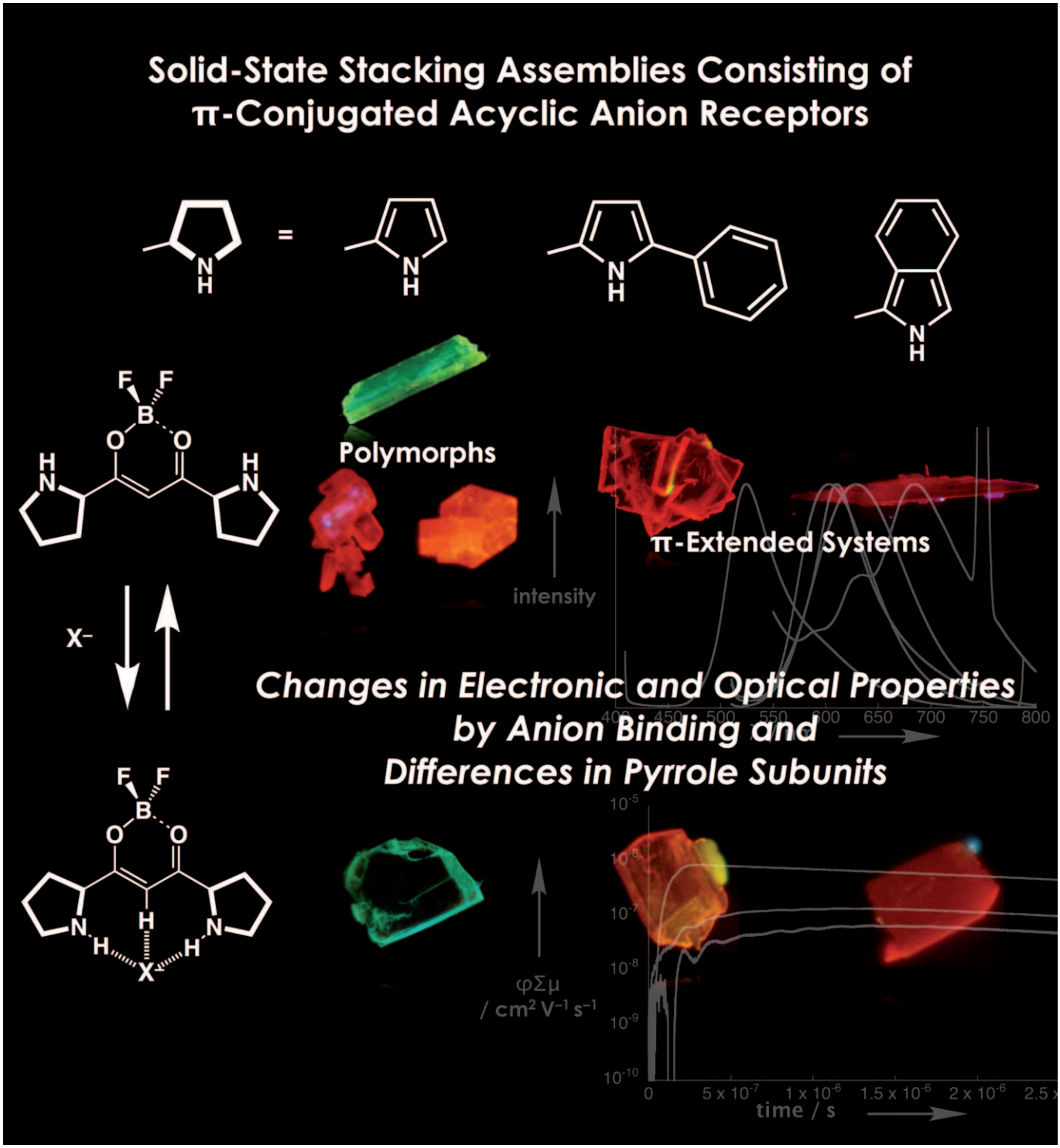

Abstract: On the basis of the chemistry in solution, the solid-state structures and the corresponding electronic and optical properties of dipyrrolyldiketone boron complexes as π-conjugated acyclic anion receptors have been investigated. Solid-state assemblies of the receptors exhibit anion-dependent properties that are in sharp contrast to those in the solution state. Anion complexation, along with structural differences in the pyrrole subunits such as a benzo-fused pyrrole, plays an essential role not only in the formation of the assembled modes but also in determining electronic and optical properties, as well as the charge-carrier mobilities. In addition, by anion complexation, inclusion of the counter cations into the crystals has also been found to be one of the essential factors to determine the properties.

Keywords: anions · crystal engineering · heterocycles · receptors · self-assembly

Introduction

Crystals, 3D molecular assemblies, are promising materials for use in field-effect transistors (FETs),[1] stimuli-responsive actuators,[2] and gas and molecular storage units.[3] These fascinating properties are derived from ordered arrangements of molecules that act as "bricks" in the crystals. Among the building blocks of crystals, π-conjugated molecules are fascinating because of their ability to form stacking structures that exhibit electronic properties that are not observed in single molecules.[4] Thus far, we have prepared acyclic π-conjugated systems, dipyrrolyldiketone boron complexes (e.g., **1** and **2**), which show anion-driven conformation changes by inversion (flipping) of two pyrrole rings in the solution state (Scheme 1).[5,6] Anion receptors based on core π planes that are substituted with aliphatic and/or hydrophilic chains have attracted much attention as building subunits of soft materials such as supramolecular gels[5b,6b] and amphiphilic vesicles.[6g] On the other hand, the absence of supplementary dimension-controlled interactions enables the anion receptors to afford crystals, wherein various assembled structures are formed. Conformational changes in the receptors as monomers by anions in the solution state are amplified to provide characteristic properties in the bulk state. In fact, representative π-conjugated anion receptors, including the newly synthesized π-extended benzo-fused receptor, **3**, have been shown to exhibit anion-driven modulations of assembled structures, electronic and optical properties, and charge-carrier mobilities in the crystals.

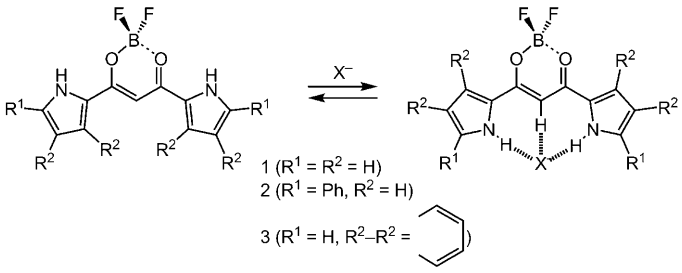

Scheme 1. Anion-responsive π-conjugated systems **1**–**3** and their anion-binding mode.

Results and Discussion

Synthesis and characterization of benzo-fused pyrrole-based anion receptors: Benzo-fused receptor **3** was obtained through the precursory ethano-bridged derivative **3′**, which was prepared by the reaction of bicyclo-[2.2.2]octadiene-fused pyrrole[7] and malonyl chloride and by subsequent treatment with $BF_3{\cdot}OEt_2$ (Scheme 2a). Photo-responsive decomposition, which is observed in **3** as well as the α-methyl-substituted derivative **3″** (Scheme 2b), in organic solvents such as CH_2Cl_2, has not been observed in the solid state. Absorption and emission maxima (λ_{em}) of **1**–**3** in CH_2Cl_2 (λ_{max} = 432,[6a] 500,[6b] and 528 nm; λ_{em} = 451,[6a] 529,[6b] and 540 nm excited at each λ_{max}) are correlated with HOMO–LUMO gaps of 3.58 (**1**),[6a] 3.08 (**2**),[6b] and 2.94 eV (**3**) calculated at the B3LYP/6-31+G(d,p)//B3LYP/6-31G(d,p) level.[8] Stokes shifts of **1**–**3** are 0.12, 0.14, and 0.052 eV, respectively, in CH_2Cl_2, suggesting that the conformations in the steady and excited states of π-extended **3** are fairly analogous in comparison with those of **1** and **2**. The receptors **1**–**3** exhibit anion-binding behavior in solution.[9] Binding constants (K_a, M^{-1}) of **3** at −50 °C estimated by ^1H NMR spec-

[a] Prof. Dr. H. Maeda, Y. Bando, Y. Haketa
College of Pharmaceutical Sciences
Institute of Science and Engineering
Ritsumeikan University, Kusatsu 525-8577 (Japan)
Fax: (+81) 77-561-2659
E-mail: maedahir@ph.ritsumei.ac.jp

[b] Prof. Dr. H. Maeda, Prof. Dr. S. Seki
PRESTO (Japan) Science and Technology Agency (JST)
Kawaguchi 332-0012 (Japan)

[c] Y. Honsho, Prof. Dr. S. Seki
Department of Applied Chemistry
Graduate School of Engineering
Osaka University, Suita 565–0871 (Japan)
Fax: (+81) 6-6879-4586
E-mail: seki@chem.eng.osaka-u.ac.jp

[d] H. Nakajima, Prof. Dr. N. Tohnai
Department of Material and Life Science
Graduate School of Engineering
Osaka University, Suita 565-0871 (Japan)
Fax: (+81) 6-6879-7404
E-mail: tohnai@mls.eng.osaka-u.ac.jp

Supporting information for this article is available on the WWW under http://dx.doi.org/10.1002/chem.201001852.

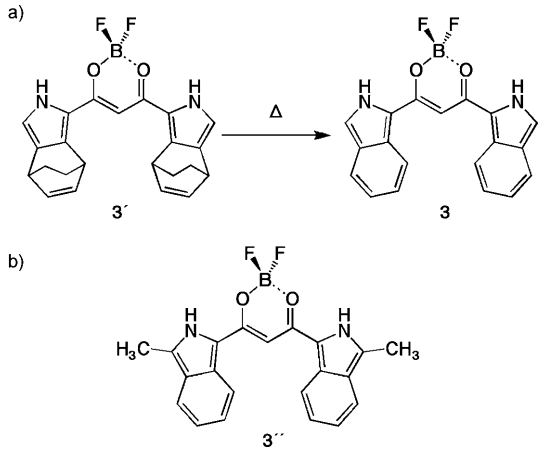

Scheme 2. a) Synthesis of **3** from **3′** through retro-Diels–Alder reaction and b) α-methyl-substituted derivative **3″**.

troscopy in CD_2Cl_2 owing to the photo-responsive properties are 83000 (Cl^-) and 7700 (Br^-) M^{-1}, which are larger than the K_a values of the β-ethyl-substituted receptor, 33000 (Cl^-) and 2500 (Br^-) M^{-1}, determined by UV/Vis absorption spectra in CH_2Cl_2. This result suggests that benzo-fusion is effective for anion binding in the solution state.[10] Upon the addition of, for example, Br^- as a tetrabutylammonium (TBA) salt, the absorption maxima of **1**–**3** hardly shift to 435, 502, and 531 nm, respectively, in CH_2Cl_2. Almost no shifts in the absorption bands upon anion binding indicate that **1**–**3** are not suitable for use as colorimetric sensors in the solution state. Fluorescence quantum yields Φ_F (and λ_{em}) of Br^- complexes of **1**–**3** are 0.78 (454 nm), 0.76 (529 nm), and 0.57 (531 nm), respectively, which are slightly decreased in **1** and **2** and are almost the same in **3** when compared to those of the free receptors **1**–**3** ($\Phi_F = 0.92$, 0.95, and 0.55, respectively).

Solid-state assemblies of the anion receptors: Single-crystal X-ray structures of **1**–**3** are shown in Figure 1. We have found the formation of polymorphism in the single crystals of **1**: Slow evaporation of a CH_2Cl_2/MeOH solution of **1** gives multicrystalline systems that include the major product **1r** (rectangular red crystal) along with yellow crystals **1y** and hexagonal-shaped vermillion crystals **1v** as minor components.[11] As already reported, vapor diffusion in the CH_2Cl_2/hexane solvent system affords only **1r**, whereas two types of stacking structures exist with *anti* orientation of BF_2 units (Figure 1a).[6a] In contrast, **1y** includes a stacking mode with BF_2 moieties oriented on the same *syn* side (Figure 1b). On the other hand, the molecules in **1v**, in which one of the pyrrole rings is inverted, form stacking structures with an *anti* orientation (Figure 1c) and also afford N–H···F–B hydrogen-bonding 1D chains. Interestingly, upon heating at 170 °C for 1 h, crystals of **1y** were transformed into reddish crystals. Variable-temperature (VT) X-ray diffraction (XRD) measurements of **1y** clearly showed the transition to the pattern of **1r** around 160 °C.[12] Further, in contrast to the *anti* orientation of phenyl-substituted **2** (Figure 1d),[6b] benzo-fused **3** afforded *syn*-oriented stacking structures in the solid state (Figure 1e).[13] The distances between approximately parallel-arranged π planes in **1r**, **1y**, **1v**, and **3** are 3.33 and 3.25/3.35 (**1r**), 3.34 (**1y**), 3.29/3.32 (**1v**), and 3.35 Å (**3**); these values may be attributed to stable and effective π–π stacking. The distances between the neighboring boron units in the stacking structures are 7.50 and 5.48/8.88 (**1r**), 4.86 (**1y**), 5.73/7.42 (**1v**), and 5.05 Å (**3**).

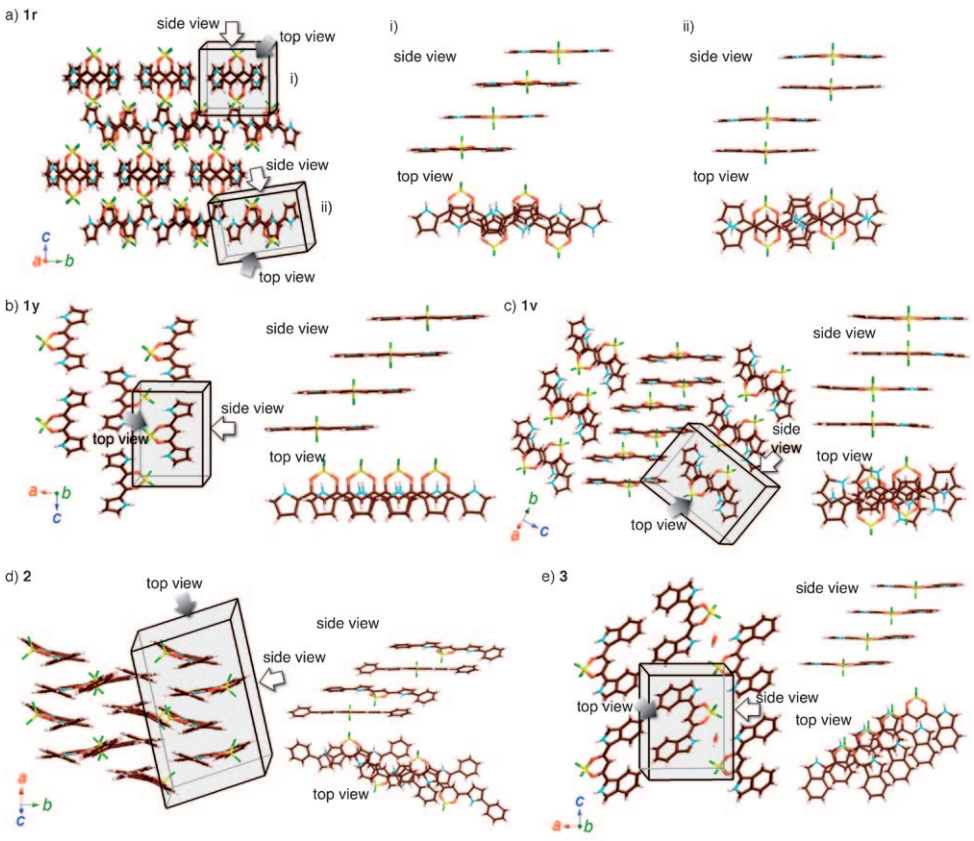

Figure 1. Solid-state stacking assemblies (packing diagrams and side and top views) of a) **1r** (two types of stacking structures i and ii),[6a] b) **1y**, c) **1v**, d) α-phenyl **2**,[6c] e) benzo-fused **3**. Atom color code: brown, pink, yellow, green, blue, and red refer to carbon, hydrogen, boron, fluorine, nitrogen, and oxygen, respectively. The arrows represent the directions of the corresponding selected views.

In contrast to these crystals, the phenyl-substituted **2** exhibited less-efficient π–π interactions with a dihedral angle of 19° between neighboring stacking π planes, which is derived from mean planes consisting of 16 core atoms.

Solid-state assemblies of the receptor-anion complexes: The receptors **1**–**3** can form crystals of receptor–anion complexes from appropriate solvents (Figure 2). Here, Br^- ions (as TBA or tetrapropylammonium (TPA) salts) were used because these salts are less deliquescent than the corresponding Cl^- crystals. Unsubstituted **1** (Figure 2a) forms a Br^--bridged crinkled 1D chain structures with N(−H)···Br and C(−H)···Br lengths of 3.34/3.30 and 3.66 Å in the solid state, in which the dihedral angle between the mean planes of neighboring receptors is 70.7°. Counter TBA cations are arranged along the aligned receptor-Br^- complexes, as observed in the corresponding Cl^- complex.[6a] On the other hand, benzo-fused **3** (Figure 2c) forms crinkled and planar Br^--bridged 1D chain structures, in which Br^- is associated with pyrrole NH (N(−H)···Br: 3.21 (*a*) and 3.37 (*b*) Å), bridging CH (C(−H)···Br: 4.28 (*c*) Å), and benzo CH units (C(−H)···Br: 3.89 (*d*) and 3.92 (*e*) Å). 2D gridlike solid-state structures, which encapsulate TBA cations inside rhombic tubes, are fabricated from the crinkled chains (Figure 2c, i), with the dihedral angle at 70.3° between the neighboring molecules and the completely parallel chains (Figure 2c, ii). The Br···Br distances within the chain structures of **1** and **3** are 9.24 and 11.72 (chain in i)/10.14 Å (chain in ii), respectively. In contrast to the α-unsubstituted **1** and **3**, α-phenyl **2** (Figure 2b) forms the regular Br^--binding complex (Figure 2b, i) with N(−H)···Br and C(−H)···Br lengths of 3.36/3.42 and 3.49 Å because of the additional interaction (C(−H)···Br: 3.68/3.68 Å) of *o*-CH sites of the aryl units. In this case, Br^- complexes are stacked with counter TPA cations to form charge-by-charge assemblies (Figure 2b, ii) comprising alternatively located charged species. The coordination mode for Br^- in **2** is quite similar to that for Cl^-,[6b] and the mean distance of the neighboring complexes in charge-by-charge stacking of **2**·Br^--TPA^+ is 7.44 Å, which is slightly larger than that for **2**·Cl^--TPA^+ (7.29 Å). In all the Br^- complexes, it is essential to focus on the aliphatic counter cations in the assembled structures on the basis of the appropriately arranged anion complexes: such cations interfere with the interactions between π-conjugated moieties of the receptor–anion complexes and, as a result, affect the physical properties of single crystals as discussed in the following sections.

Solid-state electronic and optical properties: Aggregates in the crystals of **1**–**3** exhibit distinct electronic states that

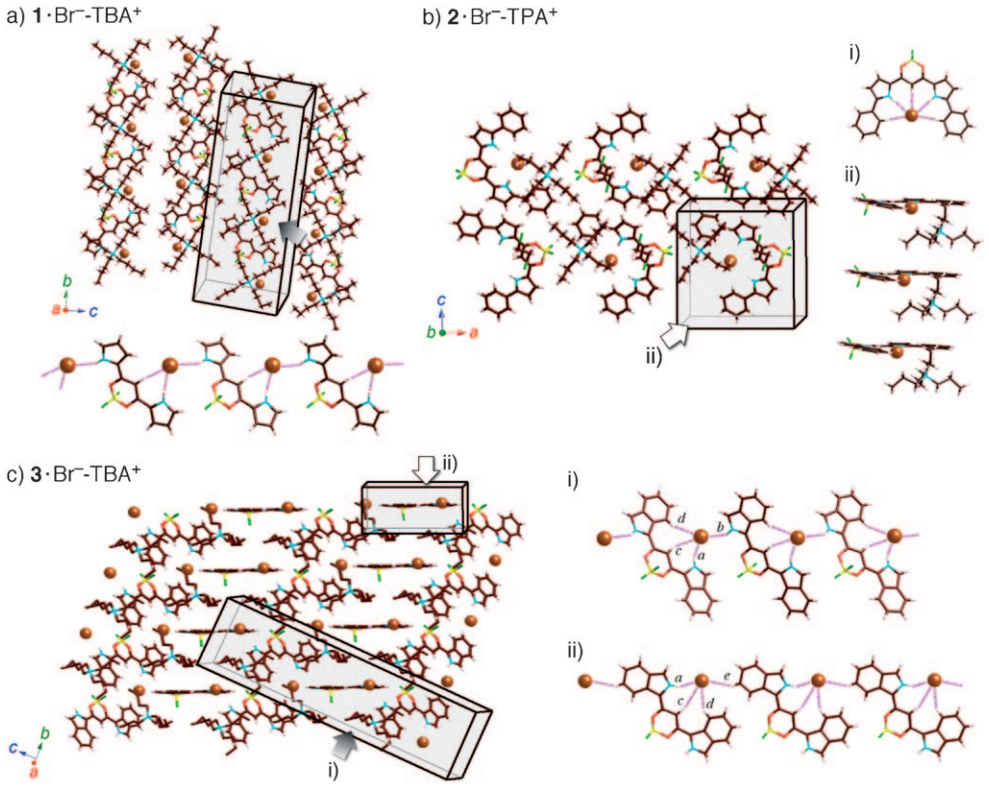

Figure 2. Solid-state structures (packing diagrams and selected views) of Br^- complexes of anion receptors **1**–**3**: a) **1** (a Br^--bridged 1D chain as a selected view); b) **2** (i: single molecule and ii: charge-by-charge stacking structure as selected views); c) **3** (i and ii: Br^--bridged 1D chains as selected views). TBA and TPA cations are omitted for clarity in the selected views except for b ii. Atom color code: brown, pink, yellow, light brown, green, blue, and red refer to carbon, hydrogen, boron, bromine, fluorine, nitrogen, and oxygen, respectively. The arrows represent the directions of the corresponding selected views.

depend on the relative configurations between neighboring molecules. Solid-state excitation and emission spectra and photographs of the crystals are shown in Figure 3. Excitation maxima are distinct for **1r** ($\lambda_{max}=522$ nm), **1y** ($\lambda_{max}=340$ and 494 nm), and **1v** ($\lambda_{max}=540$ nm), and emissions reflect these values: $\lambda_{em}=630$ (**1r**), 524 (**1y**), and 604 nm (**1v**), excited at 500 (**1r** and **1v**) and 400 nm (**1y**). In **2** and **3**, excitation and emission (excited at 500 nm) peaks are observed at 579 and 610 nm for **2** and 589 and 685 nm for **3**, respectively. In fact, the red-shift values of the excitation and emission spectra in the solid state compared to the absorption and emissions from dispersed monomers in the solution state (CH_2Cl_2) are 90 and 156 nm for **1r**, 62 and 50 nm for **1y**, 108 and 130 nm for **1v**, 79 and 81 nm for **2**, and 61 and 145 nm for **3**, respectively. These shifts correlate mainly with the arrangements of the π-conjugated molecules in the solid state. The complicated solid-state absorption and emission properties of the π-conjugated systems can be attributed to various parameters such as 1) (slight) conformational distortions derived from C–C single-bond connections between components, 2) arrangements (orientation and distance) of neighboring chromophores, and 3) interactions between stacking columnar structures. Factors 2 and 3 are related significantly to the exciton coupling between the chromophores. At present, it is difficult to estimate the transition dipole moments of the anion receptors; these would be useful for explaining the solid-state absorption and emission.

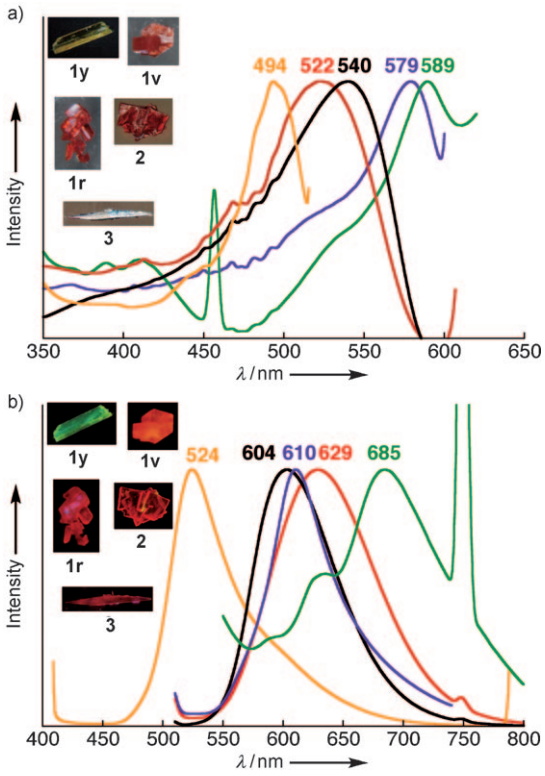

Figure 3. a) Excitation spectra corresponding to each emission maximum and b) emission spectra of the crystals of **1r** (red), **1y** (orange), **1v** (black), **2** (purple), and **3** (green). Photographs of crystals (**1r**, **1y**, **1v**, **2**, and **3**) under a) visible light and b) $UV_{365\,nm}$ light are shown in the insets.

As can be observed in Figure 4, the excitation maxima of the crystalline Br^--binding complexes are observed at $\lambda_{max}=$ 380, 450, and 468 nm (**1**·Br^--TBA^+), 406 and 560 nm (**2**·Br^--TPA^+), and 581 nm (**3**·Br^--TBA^+), suggesting that TBA or TPA cations are located between receptor–anion complexes, and therefore interfere with the π–π interactions of the π-plane chromophores. Further, solid-state fluorescence emissions of these complexes are observed at $\lambda_{em}=$ 484 and 583 nm (**1**·Br^--TBA^+), 580 nm (**2**·Br^--TPA^+), and 612 nm (**3**·Br^--TBA^+), excited at 400 nm (**1**·Br^--TBA^+) or 500 nm (**2**·Br^--TPA^+ and **3**·Br^--TBA^+). Excitation bands of **1**·Br^--TBA^+ for different emission maxima are observed at 380 and 468 nm for $\lambda_{em}=484$ nm and 450 nm for $\lambda_{em}=$ 583 nm; this result suggests that these emissions are derived from different pathways during excitation. Moderate blue shifts, as compared with the free receptors, are derived from insertion of aliphatic cations between the chromophores (receptor–anion complexes), which weakens their exciton coupling. However, red shifts (compared with the solution state) are presumably due to the edge-to-edge interactions of the receptor–anion complexes.[14]

Charge-carrier mobilities in the single crystals: Ordered stacking structures of π-conjugated molecules, as observed in the crystal structures of the anion receptors and their anion complexes, are suitable for use as charge-conductive

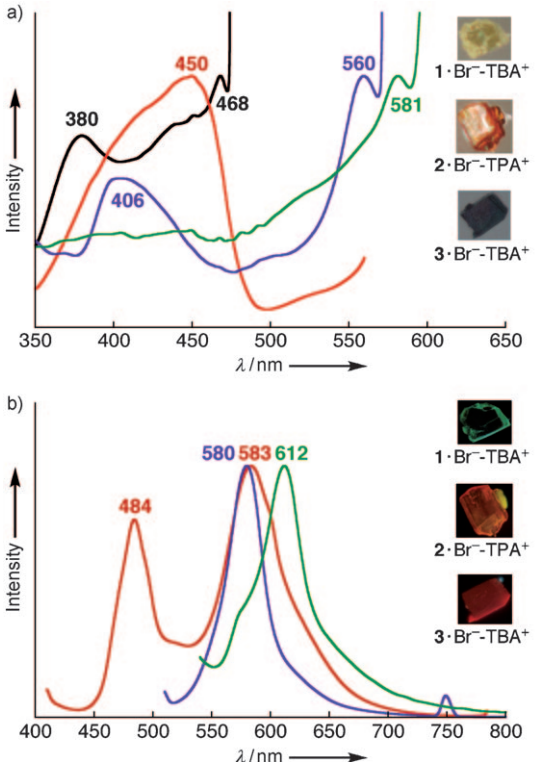

Figure 4. a) Excitation spectra corresponding to each emission maximum and b) emission spectra of the crystals of **1**·Br^--TBA^+ (red and black for $\lambda_{em}=583$ and 484 nm), **2**·Br^--TPA^+ (purple), and **3**·Br^--TBA^+ (green). Photographs of crystals (**1**·Br^--TBA^+, **2**·Br^--TPA^+, and **3**·Br^--TBA^+) under a) visible light and b) $UV_{365\,nm}$ light are shown in the insets.

materials. Therefore, we have conducted flash photolysis time-resolved microwave conductivity (FP-TRMC) measurements,[15] which allow the estimation of the behavior of mobile charge carriers along all the axes of the crystals. When a 355 nm laser pulse was applied at 25 °C, the mobilities of **1r** were determined to be 0.05, 0.02, and 0.03 $cm^2V^{-1}s^{-1}$ for the *a*, *b*, and *c* axes of the crystal, respectively. Anisotropy was observed in **1y** (0.8, 0.2, and 0.07 $cm^2V^{-1}s^{-1}$ for the *a*, *b*, and *c* axes) in contrast to **1r** and **1v** (0.7, 0.8, and 0.6 $cm^2V^{-1}s^{-1}$ for the *a*, *b*, and *c* axes). Benzo-fused **3** also shows high and anistropic conductivities (1, 0.2, and 0.06 $cm^2V^{-1}s^{-1}$ for the *a*, *b*, and *c* axes, respectively), whereas α-phenyl **2** exhibits smaller conductivities of 0.02, 0.03, and 0.05 $cm^2V^{-1}s^{-1}$ for the *a*, *b*, and *c* axes, respectively. Apparently, slipped parallel stacking of π-planes leads to high hole mobility and anistropic properties along the stacking direction (see the Supporting Information and CIF files). Further, FP-TRMC measurements of Br^- complexes show conductivities of 7×10^{-3}, 8×10^{-3}, and 3×10^{-4} $cm^2V^{-1}s^{-1}$ (**1**·Br^--TBA^+) and 4×10^{-3}, 4×10^{-3}, and 7×10^{-4} $cm^2V^{-1}s^{-1}$ (**2**·Br^--TPA^+) for the *a*, *b*, and *c* axes of the crystals, and 8×10^{-3} and 7×10^{-3} $cm^2V^{-1}s^{-1}$ (**3**·Br^--TBA^+) for the *a* and *c* axes of the crystal, respectively. Therefore, crystals of Br^- complexes as tetraalkylammonium salts give smaller conductivities than those of anion-free crystals.

Conclusion

We have demonstrated substituent- and anion-dependent properties of π-conjugated acyclic anion receptors in the solid state. Anion complexation, along with differences in pyrrole subunits such as a benzo-fused core, plays an essential role not only in the formation of assembled structures but also in determining the electronic and optical properties. In particular, some crystals show high charge-carrier mobilities with large anistropy. The molecular systems reported herein are fairly complicated, so at present it is not easy to discuss the correlation between assembled structures and their fascinating properties. However, we are currently investigating how the choice of receptors, anions, and cations affects the assembly and the useful properties of crystals and soft materials.

Experimental Section

General methods and materials: Starting materials were purchased from Wako, Nacalai, and Aldrich and were used without further purification unless otherwise stated. UV/Vis spectra were recorded on a Hitachi U-3500 spectrometer. Fluorescence spectra and quantum yields were recorded on a Hitachi F-4500 fluorescence spectrometer for ordinary solutions and a Hamamatsu Quantum Yields Measurements System for Organic LED Materials C9920–02, respectively. The NMR spectra that were used in the characterization of the products were recorded on a JEOL ECA-600 600 MHz spectrometer. All NMR spectra were referenced to the solvent. Matrix-assisted laser desorption ionization time-of-flight mass spectrometries (MALDI-TOF-MS) were recorded on a Shimadzu Axima-CFRplus using negative mode. TLC analyses were carried out on aluminum sheets coated with silica gel 60 (Merck 5554). Column chromatography was performed on Sumitomo alumina KCG-1525, Wakogel C-200, C-300, and Merck silica gel 60 and 60H.

1,3-Bis-(4,7-ethano-4,7-dihydroisoindol-1-yl)-1,3-propanedione: A CH_2Cl_2 solution (50 mL) of 4,7-ethano-4,7-dihydroisoindole[7] (250.0 mg, 1.72 mmol) was treated with malonyl chloride (121.4 mg, 0.86 mmol) under nitrogen at 0 °C and was stirred for 45 min at the same temperature. After confirming the consumption of the starting pyrrole by TLC analysis, the mixture was washed with a saturated aqueous solution of Na_2CO_3 and water, dried over anhydrous Na_2SO_4, filtered, and evaporated to dryness. The residue was then chromatographed over a silica-gel column (Wakogel C-300, eluent: 3% MeOH/CH_2Cl_2) and recrystallized from CH_2Cl_2/hexane to afford 1,3-bis-(4,7-ethano-4,7-dihydroisoindol-1-yl)-1,3-propanedione (306.7 mg, 50%) as a pale-yellow solid. R_f=0.43 (3% MeOH/CH_2Cl_2); ^{1}H NMR (600 MHz, $CDCl_3$, 20 °C; the diketone was obtained as a mixture of keto and enol tautomers in the ratio of 1:0.40): keto form δ=8.83 (br, 2H; NH), 6.68 (d, J=2.4 Hz, 2H; pyrrole-H), 6.57–6.47 (m, 4H; olefin-H), 4.48 (s, 2H; CH_2), 4.32–4.24 (m, 2H; bridgehead-H), 3.92–3.90 (m, 2H; bridgehead-H), 1.70–1.43 ppm (m, 8H; CH_2CH_2); enol form δ=16.79 (br, 1H; OH), 8.58 (s, 2H; NH), 6.67 (d, J=2.4 Hz, 2H; pyrrole-H), 6.57–6.47 (m, 4H; olefin-H), 6.40 (s, 1H; CH), 4.32–4.24 (m, 2H; bridgehead-H), 3.92–3.90 (m, 2H; bridgehead-H), 1.70–1.43 ppm (m, 8H; CH_2CH_2); MALDI-TOF-MS: *m*/*z* (%): calcd for $C_{23}H_{21}N_2O_2$: 357.16 $[M-H]^-$; found: 357.2 (100), 358.2 (25).

BF_2 complex of 1,3-bis-(4,7-ethano-4,7-dihydroisoindol-1-yl)-1,3-propanedione, 3′: BF_3·OEt_2 (791.9 mg, 5.58 mmol) was added to a solution of 1,3-bis-(4,7-ethano-4,7-dihydroisoindol-1-yl)-1,3-propanedione (101.5 mg, 0.28 mmol) in CH_2Cl_2 (20 mL) and was stirred for 20 min at room temperature. After removal of the solvent, silica-gel column chromatography (Wakogel C-300, eluent: 3% and 0.5% MeOH/CH_2Cl_2), and crystallization from CH_2Cl_2/hexane afforded **3′** (84.6 mg, 74%) as an orange solid. R_f=0.30 (0.5% MeOH/CH_2Cl_2); ^{1}H NMR (600 MHz, $CDCl_3$, 20 °C): δ= 8.84 (br, 2H; NH), 6.83–6.82 (m, 2H; pyrrole-H), 6.65 (s, 1H; CH), 6.59–6.55 (m, 4H; olefin-H), 4.32–4.31 (m, 2H; bridgehead-H), 3.98–3.96 (m, 2H; bridgehead-H), 1.76–1.43 ppm (m, 8H; CH_2CH_2); UV/Vis (CH_2Cl_2): λ_{max} ($\varepsilon\times10^{-5}$)=449.0 nm (1.05 $M^{-1}cm^{-1}$); MALDI-TOF-MS: *m*/*z* (%): calcd for $C_{23}H_{20}BF_2N_2O_2$: 405.16 $[M-H]^-$; found: 405.2 (57), 406.2 (100). This compound was further characterized by X-ray diffraction analysis.

BF_2 complex, 3: A CH_2Cl_2 solution (80 mL) of **3′** (30.5 mg, 0.075 mmol) was evaporated and the residue was heated under vacuum (0.75 mm Hg) at 153–166 °C for 3.7 h. Flash silica-gel column chromatography (eluent: 3% MeOH/CH_2Cl_2) and crystallization from 10% MeOH/CH_2Cl_2 and hexane afforded **3** (19.8 mg, 75%) as a deep-green solid. R_f=0.22 (3% MeOH/CH_2Cl_2); ^{1}H NMR (600 MHz, [D_6]DMSO, 60 °C): δ=13.72 (br, 2H; NH), 8.33 (d, J=7.8 Hz, 2H; Ar-H), 8.10 (s, 2H; pyrrole-H), 7.87 (t, J=8.4 Hz, 2H; Ar-H), 7.47 (t, J=7.2 Hz, 2H; Ar-H), 7.26 (t, J=7.8 Hz, 4H; Ar-H), 7.05 ppm (s, 1H; CH); UV/Vis (CH_2Cl_2): λ_{max} ($\varepsilon\times10^{-5}$)= 528.0 nm (1.38 $M^{-1}cm^{-1}$); MALDI-TOF-MS: *m*/*z* (%): calcd for $C_{19}H_{12}BF_2N_2O_2$: 349.10 $[M-H]^-$; found: 348.1 (51), 349.1 (100). This compound was further characterized by X-ray diffraction analysis.

1,3-Bis-(4,7-ethano-4,7-dihydro-3-methylisoindol-1-yl)-1,3-propanedione: A solution of 4,7-ethano-4,7-dihydro-3-methylisoindole[16] (383.2 mg, 2.41 mmol) in $CHCl_3$ (120 mL) was treated with malonyl chloride (203.5 mg, 1.44 mmol) at 0 °C and was stirred for 1 h at the same temperature. After confirming the consumption of the starting pyrrole by TLC analysis, the mixture was washed with a saturated aqueous solution of Na_2CO_3, water, and brine, dried over anhydrous Na_2SO_4, filtered, and evaporated to dryness. The residue was then chromatographed over a silica-gel column (Wakogel C-300, eluent: 5% MeOH/CH_2Cl_2) and was recrystallized from CH_2Cl_2/hexane to afford 1,3-bis-(4,7-ethano-4,7-dihydro-3-methylisoindol-1-yl)-1,3-propanedione (110.2 mg, 38%) as a pale-yellow solid. R_f=0.53 (5% MeOH/CH_2Cl_2); ^{1}H NMR (600 MHz, $CDCl_3$, 20 °C; diketone is obtained as a keto tautomer): δ=8.44 (br, 2H; NH), 6.52 (s, 2H; olefin-H), 6.48 (s, 2H; olefin-H), 4.47–4.17 (m, 4H; CH_2+ bridgehead-H), 3.82–3.81 (m, 2H; bridgehead-H), 2.22 (s, 6H; CH_3), 1.59–1.40 ppm (m, 8H; CH_2CH_2); MALDI-TOF-MS: *m*/*z* (%): calcd for $C_{26}H_{25}N_2O_2$: 385.19 $[M-H]^-$; found: 385.2 (100), 386.2 (29).

BF_2 complex of 1,3-bis-(4,7-ethano-4,7-dihydro-3-methylisoindol-1-yl)-1,3-propanedione: $BF_3{\cdot}OEt_2$ (141.9 mg, 1.00 mmol) was added to a solution of 1,3-bis-(4,7-dihydro-4,7-ethano-3-methylisoindol-1-yl)-1,3-propanedione (77.3 mg, 0.20 mmol) in CH_2Cl_2 (20 mL) and was stirred for 20 min at room temperature. After removal of the solvent, silica-gel column chromatography (Wakogel C-300, eluent: 1% and 0.5% MeOH/CH_2Cl_2) and crystallization from THF/hexane afforded the BF_2 complex (64.1 mg, 74%) as a yellow solid. R_f=0.60 (6% MeOH/CH_2Cl_2), ^{1}H NMR (600 MHz, $CDCl_3$, 20°C): δ=8.62 (br, 2H; NH), 6.58 (t, J=7.2 Hz, 2H; olefin-H), 6.53 (s+t, J=7.8 Hz, 3H; CH+olefin-H), 4.26 (br, 2H; bridgehead-H), 3.89 (br, 2H; bridgehead-H), 2.29 (s, 6H; CH_3), 1.72–1.42 ppm (m, 8H; CH_2CH_2); UV/Vis (CH_2Cl_2): λ_{max} ($\varepsilon\times10^{-5}$)= 470.0 nm (0.77 $M^{-1}cm^{-1}$); MALDI-TOF-MS: m/z (%): calcd for $C_{25}H_{24}BF_2N_2O_2$: 433.19 $[M-H]^-$; found: 433.2 (42), 434.2 (100).

BF_2 complex 3″: A CH_2Cl_2 solution of the BF_2 complex of 1,3-bis-(4,7-ethano-4,7-dihydro-3-methylisoindol-1-yl)-1,3-propanedione (25.0 mg, 0.058 mmol) was evaporated and the residue was heated under vacuum (0.75–1.50 mmHg) at 160–181°C for 3.3 h. Silica-gel column chromatography (Wakogel C-300, eluent: 3% THF/CH_2Cl_2) and crystallization from THF/hexane afforded **3″** (16.3 mg, 75%) as a black solid. R_f=0.32 (3% THF/CH_2Cl_2); ^{1}H NMR (600 MHz, [D$_6$]DMSO, 70°C): δ=13.32 (br, 2H; NH), 8.25 (d, J=7.2 Hz, 2H; Ar-H), 7.84 (d, J=7.8 Hz, 2H; Ar-H), 7.46 (t, J=6.6 Hz, 2H; Ar-H), 7.21 (dd, J=7.8 and 6.6 Hz, 2H; Ar-H), 6.86 (s, 1H; CH), 2.75 ppm (s, 6H; CH_3); UV/Vis (CH_2Cl_2): λ_{max} ($\varepsilon\times10^{-5}$)=546.5 nm (1.26 $M^{-1}cm^{-1}$); MALDI-TOF-MS: m/z (%): calcd for $C_{21}H_{16}BF_2N_2O_2$: 377.13 $[M-H]^-$; found: 377.0 (100), 378.0 (78). This compound was further characterized by X-ray diffraction analysis.

Single-crystal X-ray analysis: All the data were collected at 123 K on a Rigaku RAXIS-RAPID diffractometer with graphite monochromated $Mo_{K\alpha}$ radiation (λ=0.71075 Å). The structures were solved by direct methods.

*Complex **1y***: A single crystal of **1y** was obtained by slow evaporation of a MeOH/CH_2Cl_2 solution of **1**. The crystal was a red-colored prism of approximate dimensions 0.40×0.20×0.10 mm. Crystal data for **1y** (from CH_2Cl_2/MeOH): $C_{11}H_9BF_2N_2O_2$, M_r=250.01; monoclinic; $C2/c$ (no. 15); a=23.749(19), b=4.855(3), c=18.380(11) Å; β=95.83(3)°; V=2108(2) Å^3; T=123(2) K; Z=8; ρ_{cald}=1.575 g cm^{-3}; $\mu(Mo_{K\alpha})$=0.131 mm^{-1}; R_1=0.0601; wR_2=0.1581; GOF=1.056 [$I>2\sigma(I)$].

*Complex **1v***: A single crystal of **1v** was obtained by slow evaporation of a MeOH/CH_2Cl_2 solution of **1**. The crystal was a red-colored prism of approximate dimensions 0.50×0.20×0.20 mm. Crystal data for **1v** (from CH_2Cl_2/MeOH): $C_{11}H_9BF_2N_2O_2$, M_r=250.01; monoclinic; $C2/c$ (no. 15); a=11.882(7), b=8.945(4), c=20.144(9) Å; β=90.24(2); V=2141.0(18) Å^3; T=123(2) K; Z=8; ρ_{cald}=1.551 g cm^{-3}; $\mu(Mo_{K\alpha})$=0.129 mm^{-1}; R_1=0.0334; wR_2=0.0897; GOF=1.080 [$I>2\sigma(I)$].

*Complex **3***: A single crystal of **3** was obtained by vapor diffusion of hexane into a THF solution of **3**. The crystal was a purple-colored prism of approximate dimensions 0.70×0.20×0.10 mm. Crystal data for **3** (from THF/hexane): $C_{19}H_{14}BF_2N_2O_{2.50}$; M_r=359.13; monoclinic; $C2/c$ (no. 15); a=29.257(16), b=5.049(2), c=21.734(9) Å; β=90.33(2)°; V=3210(3) Å^3; T=123(2) K; Z=8; ρ_{cald}=1.486 g cm^{-3}; $\mu(Mo_{K\alpha})$=0.114 mm^{-1}; R_1=0.0388; wR_2=0.0986; GOF=1.079 [$I>2\sigma(I)$].

*Complex **3′***: A single crystal of **3′** was obtained by vapor diffusion of hexane into a solution of **3′** in CH_2ClCH_2Cl. The crystal was a red-colored prism of approximate dimensions 0.40×0.20×0.10 mm. Crystal data for **3′** (from CH_2ClCH_2Cl/hexane): $C_{25}H_{21}BF_2N_2O_2$; M_r=406.23, monoclinic; $P2_1/n$ (no. 14); a=9.257(3), b=9.476 (3), c=21.811 (6) Å; β=100.019 (14)°; V=1884.1 (10) Å^3; T=123(2) K; Z=4; ρ_{cald}=1.432 g cm^{-3}; $\mu(Mo_{K\alpha})$=0.104 mm^{-1}; R_1=0.0449; wR_2=0.1076; GOF=1.052 [$I>2\sigma(I)$].

*Complex **3″***: A single crystal of **3″** was obtained by vapor diffusion of hexane into a solution of **3″** in THF. The data crystal was a purple-colored prism of approximate dimensions 0.50×0.50×0.30 mm. Crystal data for **3″** (from THF/hexane): $C_{21}H_{17}BF_2N_2O_2{\cdot}2C_4H_8O$; M_r=359.13; orthorhombic; *Pbca* (no. 61); a=11.731 (4), b=17.327 (6), c=25.249 (10) Å; V=5132 (3) Å^3; T=123(2) K; Z=8; ρ_{cald}=1.342 g cm^{-3}; $\mu(Mo_{K\alpha})$=0.098 mm^{-1}; R_1=0.0673; wR_2=0.1687; GOF=0.983 [$I>2\sigma(I)$].

*Complex **1**·TBABr*: A single crystal of **1**·TBABr was obtained by vapor diffusion of hexane into a CH_2ClCH_2Cl solution of the equivalent mixture of **1** and TBABr. The crystal was a purple-colored prism of approximate dimensions 0.15×0.10×0.05 mm. Crystal data for **1**·TBABr (from CH_2ClCH_2Cl/hexane): $C_{11}H_9BF_2N_2O_2{\cdot}C_{16}H_{36}NBr{\cdot}0.5C_2H_4Cl_2$; M_r= 621.86; orthormbic; $Pbc2_1$ (no. 29); a=8.6523(19), b=18.430(3), c=39.977(7) Å; V=6375(2) Å^3; T=123(2) K; Z=8; ρ_{cald}=1.296 g cm^{-3}; $\mu(Mo_{K\alpha})$=1.413 mm^{-1}; R_1=0.0623; wR_2=0.1476; GOF=1.050 [$I>2\sigma(I)$].

*Complex **2**·TPABr*: A single crystal of **2**·TPABr was obtained by vapor diffusion of hexane in to a solution of an equivalent mixture of **2** and TPABr in CH_2ClCH_2Cl. The crystal was a purple-colored prism of approximate dimensions 0.50×0.30×0.20 mm. Crystal data for **2**·TPABr (from CH_2ClCH_2Cl/hexane): $C_{23}H_{17}BF_2N_2O_2{\cdot}C_{12}H_{28}NBr{\cdot}C_2H_4Cl_2$; M_r= 767.41; monoclinic; $P2_1/n$ (no. 14); a=12.86(3), b=8.673(12), c=35.50(5) Å; β=92.46(7)°; V=3957(11) Å^3; T=123(2) K; Z=4; ρ_{cald}=1.288 g cm^{-3}; $\mu(Mo_{K\alpha})$=1.218 mm^{-1}; R_1=0.1130; wR_2=0.2985; GOF=1.045 [$I>2\sigma(I)$].

*Complex **3**·TBABr*: A single crystal of **3**·TBABr was obtained by vapor diffusion of hexane into an acetone solution of equivalent mixture of **3** and TBABr. The data crystal was a purple-colored prism of approximate dimensions 0.20×0.10×0.10 mm. Crystal data for **3**·TBABr (from acetone/hexane): $C_{13}H_{19}B_2F_2N_2O_2{\cdot}C_{16}H_{36}NBr$; M_r=581.00; monoclinic; Cc (no. 9); a=21.582(10), b=9.144(5), c=18.258(9) Å; β=94.507(10); V=3592(3) Å^3; T=123(2) K; Z=4; ρ_{cald}=1.196 g cm^{-3}; $\mu(Mo_{K\alpha})$=1.186 mm^{-1}; R_1=0.1196; wR_2=0.3076; GOF=1.086 [$I>2\sigma(I)$].

In each case, the non-hydrogen atoms were refined anisotropically. The calculations were performed by using the crystal structure crystallographic software package of Molecular Structure Corporation.[17] CCDC-760818 (**1y**), 760819 (**1v**), 760820 (**3**), 760821 (**3′**), 760822 (**3″**), 760823 (**1**·TBABr), 760824 (**2**·TPABr), and 760825 (**3**·TBABr) contain the supplementary crystallographic data for this paper. These data can be obtained free of charge from The Cambridge Crystallographic Data Centre via www.ccdc.cam.ac.uk/data_request/cif.

DFT calculations: Ab initio calculations of **3a** and its Cl^- binding complexes were carried out by using the Gaussian 03 program[8] and an HP Compaq dc5100 SFF computer. The structures were optimized, and the total electronic energies were calculated at the B3LYP level by using a 6–31G** basis set for the receptors and [1+1] anion complexes.

Single-crystal fluorescence and excitation spectra: Fluorescence spectra and excitation spectra measurements were performed by using a FP-6500 spectrofluorometer (JASCO). The sample crystals for the measurements in the solid state were encapsulated in a quartz cell (30×30×0.3 mm) under deoxygenated conditions. The excitation wavelength was 350 nm in the fluorescence spectra measurements.

Time-resolved microwave conductivity measurements: The nanosecond laser pulses from a Nd:YAG laser (third harmonic generation, THG (355 nm) from Spectra Physics, INDY-HG (FWHM 5–8 ns) were used as excitation sources. The power density of the laser was set at 2.6–41 mJ cm^{-2} (0.47–7.3×10^{16} photons cm^{-2}). For time-resolved microwave conductivity (TRMC) measurements, the microwave frequency and power were set at ≈9.1 GHz and 3 mW respectively, so that the motion of charge carriers could not be disturbed by the low electric field of the microwave. The TRMC signal picked up by a diode (rise time <1 ns) was monitored by a digital oscilloscope. All of the above experiments were carried out at room temperature. The transient photoconductivity ($\Delta\sigma$) of the samples was related to the reflected microwave power ($\Delta P_r/P_r$) and the sum of the mobilities of charge carriers by [Eq. (1)] and [Eq. (2)], in which A, e, ϕ, N, and $\Sigma\mu$ are the sensitivity factor, the elementary charge of an electron, the photo carrier generation yield (quantum efficiency), the number of absorbed photons per unit volume, and the sum of mobilities for negative and positive carriers, respectively.[18]

$$<\Delta\sigma>=\frac{1}{A}\frac{\Delta P_r}{P_r} \quad (1)$$

$$\Delta\sigma = eN\phi\sum\mu \quad (2)$$

The polarization of the laser pulses was isotropic. All crystals were mounted on quartz rods and were coated with poly(methylmethacrylate) (PMMA). The number of photons absorbed by the crystals was estimated by the direct measurement of transmitted power of laser pulses through (quartz rod)–(crystal with PMMA binder)–(quartz rod) geometry with Opher NOVA-display laser power meter (also see the Supporting Information). The quartz rod was rotated in the microwave cavity, and the changes in the effective electric field in the crystals by the rotation of the samples were calibrated based on the geometry of the crystals captured by the digital CCD camera. Because of the small size of the crystals (the maximum length of the axes was less than 1 mm), the calibration factors for the effective field strength were estimated to be less than 0.075, which is smaller than the experimental errors originated from the measurement of the number of absorbed photons (the error factor in the number was 0.2).

The values of the conductivity in the figures were already converted into the values of $\phi\Sigma\mu$ in [Eq. (2)] based on the number of absorbed photons estimated by the above procedure. The values of ϕ in the compounds were determined by conventional DC current integration in a vacuum chamber ($<10^{-5}$ Pa) by using a crystal placed onto an inter-digitated Au electrode with 5 μm gap under excitation at 355 nm with the power density of 1.6×10^{16} photons cm^{-2}. The transient current was predominantly observed under the applied negative bias of 2–16 V ($\approx$0.4–3.2$\times10^{4}$ V cm^{-1}), and was monitored by a Tektronic TDS 350 digitizing oscilloscope with the terminate resistance ranging from 300–3 kΩ and a Keithley R6487 current integrator. The observed current transients under a variety of bias voltage crystals are represented in the Supporting Information. The other details of the apparatus were described elsewhere.[19]

Powder X-ray diffraction: Powder XRD patterns were measured by a Rigaku RINT-2000 and a Rigaku Ultima IV multipurpose X-ray diffraction system using graphite-monochromatized $Cu_{K\alpha}$ radiation ($\lambda=$ 1.54178 Å) at room temperature.

Acknowledgements

This work was supported by Grants-in-Aid for Young Scientists (B) (No. 21750155) and for Scientific Research in a Priority Area "Super-Hierarchical Structures" (No. 19022036) from the Ministry of Education, Culture, Sports, Science and Technology (MEXT) and Ritsumeikan Global Innovation Research Organization (R-GIRO) project (2008–2013). The authors thank Prof. Atsuhiro Osuka, Dr. Yasuhide Inokuma, and Dr. Shohei Saito, Kyoto University, for the X-ray analyses, and Prof. Hitoshi Tamiaki, Ritsumeikan University, for various measurements. Y.H. and Y.H. thank JSPS for a Research Fellowship for Young Scientists.

[1] a) A. R. Murphy, J. M. J. Fréchet, *Chem. Rev.* **2007**, *107*, 1066–1096; b) M. Mas-Torrent, C. Rovira, *Chem. Soc. Rev.* **2008**, *37*, 827–838.

[2] a) J. M. Sansiñena, V. Olazábal, T. F. Otero, C. N. P. da Fonseca, M.-A. De Paoli, *Chem. Commun.* **1997**, 2217–2218; b) S. Kobatake, S. Takami, H. Muto, T. Ishikawa, M. Irie, *Nature* **2007**, *446*, 778–781; c) M. Yamada, M. Kondo, R. Miyasato, Y. Naka, J. Mamiya, M. Kinoshita, A. Shishido, Y. Yu, C. J. Barrettc, T. Ikeda, *J. Mater. Chem.* **2009**, *19*, 60–62.

[3] a) S. Kitagawa, R. Matsuda, *Coord. Chem. Rev.* **2007**, *251*, 2490–2509; b) Y. Kubota, M. Takata, T. C. Kobayashi, S. Kitagawa, *Coord. Chem. Rev.* **2007**, *251*, 2510–2521.

[4] C. A. Hunter, K. R. Lawson, J. Perkins, C. J. Urch, *J. Chem. Soc. Perkin Trans. 2* **2001**, 651–669.

[5] a) H. Maeda, *Eur. J. Org. Chem.* **2007**, 5313–5325; b) H. Maeda, *Chem. Eur. J.* **2008**, *14*, 11274–11282; c) H. Maeda, *J. Inclusion Phenom. Macrocyclic Chem.* **2009**, *64*, 193–214; d) H. Maeda in *Handbook of Porphyrin Science, Vol. 8* (Eds.: K. M. Kadish, K. M. Smith, R. Guilard), World Scientific, New Jersey, **2010**, Chapter 38; e) H. Maeda, *Top. Heterocycl. Chem.* **2010**, *24*, 103–144.

[6] a) H. Maeda, Y. Kusunose, *Chem. Eur. J.* **2005**, *11*, 5661–5666; b) H. Maeda, Y. Haketa, T. Nakanishi, *J. Am. Chem. Soc.* **2007**, *129*, 13661–13674; c) H. Maeda, Y. Kusunose, Y. Mihashi, T. Mizoguchi, *J. Org. Chem.* **2007**, *72*, 2612–2616; d) H. Maeda, M. Terasaki, Y. Haketa, Y. Mihashi, Y. Kusunose, *Org. Biomol. Chem.* **2008**, *6*, 433–436; e) H. Maeda, Y. Fujii, Y. Mihashi, *Chem. Commun.* **2008**, 4285–4287; f) H. Maeda, Y. Haketa, *Org. Biomol. Chem.* **2008**, *6*, 3091–3095; g) H. Maeda, Y. Mihashi, Y. Haketa, *Org. Lett.* **2008**, *10*, 3179–3182; h) H. Maeda, Y. Ito, Y. Haketa, N. Eifuku, E. Lee, M. Lee, T. Hashishin, K. Kaneko, *Chem. Eur. J.* **2009**, *15*, 3706–3719; i) H. Maeda, Y. Haketa, Y. Bando, S. Sakamoto, *Synth. Met.* **2009**, *159*, 792–796; j) H. Maeda, N. Eifuku, *Chem. Lett.* **2009**, *38*, 208–209; k) H. Maeda, R. Fujii, Y. Haketa, *Eur. J. Org. Chem.* **2010**, 1469–1482; l) H. Maeda, Y. Terashima, Y. Haketa, A. Asano, Y. Honsho, S. Seki, M. Shimizu, H. Mukai, K. Ohta, *Chem. Commun.* **2010**, *46*, 4559–4561; m) H. Maeda, M. Takayama, K. Kobayashi, H. Shinmori, *Org. Biomol. Chem.* **2010**, *8*, DOI: 10.1039/c0ob00044b.

[7] T. Okujima, N. Komobuchi, N. Ono, *Heterocycles* **2006**, *67*, 255–267.

[8] Gaussian 03, Revision C.01, M. J. Frisch, G. W. Trucks, H. B. Schlegel, G. E. Scuseria, M. A. Robb, J. R. Cheeseman, J. A. Montgomery, Jr., T. Vreven, K. N. Kudin, J. C. Burant, J. M. Millam, S. S. Iyengar, J. Tomasi, V. Barone, B. Mennucci, M. Cossi, G. Scalmani, N. Rega, G. A. Petersson, H. Nakatsuji, M. Hada, M. Ehara, K. Toyota, R. Fukuda, J. Hasegawa, M. Ishida, T. Nakajima, Y. Honda, O. Kitao, H. Nakai, M. Klene, X. Li, J. E. Knox, H. P. Hratchian, J. B. Cross, C. Adamo, J. Jaramillo, R. Gomperts, R. E. Stratmann, O. Yazyev, A. J. Austin, R. Cammi, C. Pomelli, J. W. Ochterski, P. Y. Ayala, K. Morokuma, G. A. Voth, P. Salvador, J. J. Dannenberg, V. G. Zakrzewski, S. Dapprich, A. D. Daniels, M. C. Strain, O. Farkas, D. K. Malick, A. D. Rabuck, K. Raghavachari, J. B. Foresman, J. V. Ortiz, Q. Cui, A. G. Baboul, S. Clifford, J. Cioslowski, B. B. Stefanov, G. Liu, A. Liashenko, P. Piskorz, I. Komaromi, R. L. Martin, D. J. Fox, T. Keith, M. A. Al-Laham, C. Y. Peng, A. Nanayakkara, M. Challacombe, P. M. W. Gill, B. Johnson, W. Chen, M. W. Wong, C. Gonzalez, J. A. Pople, Gaussian, Inc., Wallingford CT, **2004**.

[9] a) *Supramolecular Chemistry of Anions* (Eds.: A. Bianchi, K. Bowman-James, E. García-España), Wiley-VCH, Weinheim, **1997**; b) *Fundamentals and Applications of Anion Separations* (Eds.: R. P. Singh, B. A. Moyer), Kluwer Academic/Plenum Publishers, New York, **2004**; c) "Anion Sensing": *Top. Curr. Chem.* **2005**, *255*, 1–238; d) J. L. Sessler, P. A. Gale, W.-S. Cho, *Anion Receptor Chemistry*, RSC, Cambridge, **2006**; e) *Recognition of Anions* (Ed.: R. Vilar), Springer, Berlin, **2008**.

[10] The K_a values of **1**, **2**, and the β-ethyl-substituted derivative in CH_2Cl_2 at RT are summarized in Ref. [6d], [6b], and [6c], respectively.

[11] Conditions to obtain the desired crystals are now under investigation; for example, reprecipitation by addition of hexane to a solution of **1** in CH_2Cl_2 affords **1y** and **1v** as major products but as small crystals.

[12] a) The details of transition mechanism are now under investigation; b) Grinding the mixtures of red and yellow precipitates (small crystals) of **1** obtained by rapid crystallization from CH_2Cl_2/hexane also exhibits the transitions from **1y** to **1r**, which were suggested by changes in the XRD patterns. The transition mechanism is now being examined.

[13] Single-crystal X-ray analyses for **3′** and **3″** have also been performed (see the Supporting Information).

[14] Crystals of the receptors **1**–**3** are responsive to tetraalkylammonium salts of the anion by grinding without solvents. Solid-state UV/Vis and fluorescence spectra of the mixtures of the receptors and 1 equiv of TBABr for **1** and **3** and TPABr for **2** exhibit 369 and 489 nm for **1**, 571 and 611 nm for **2**, and 579 and 609 nm for **3**, respectively (see the Supporting Information). Blue-shifted absorption bands of the ground mixtures compared to those of the corresponding free receptors suggest the possibility of association with anion or molecular-level interaction with TBABr or TPABr by grinding. This

behavior is also supported by the XRD patterns of the ground mixtures of **1** and **2**, which differ from those of the corresponding single crystals of the Br^- complexes of **1** and **2**. In contrast, the XRD pattern of the ground mixture of **3** is similar to the corresponding single crystal of the Br^- complex (see the Supporting Information).

[15] a) Y. Yamamoto, T. Fukushima, Y. Suna, N. Ishii, A. Saeki, S. Seki, S. Tagawa, M. Taniguchi, T. Kawai, T. Aida, *Science* **2006**, *314*, 1761–1764; b) Y. Yamamoto, T. Fukushima, A. Saeki, S. Seki, S. Tagawa, N. Ishii, T. Aida, *J. Am. Chem. Soc.* **2007**, *129*, 9276–9277; c) W. S. Li, Y. Yamamoto, T. Fukushima, A. Saeki, S. Seki, S. Tagawa, H. Masunaga, S. Sasaki, M. Takata, T. Aida, *J. Am. Chem. Soc.* **2008**, *130*, 8886–8887.

[16] Z. Shen, H. Röhr, K. Rurack, H. Uno, M. Spieles, B. Schulz, G. Reck, N. Ono, *Chem. Eur. J.* **2004**, *10*, 4853–4871.

[17] CrystalStructure: Crystal Structure Analysis Package, Rigaku and Rigaku/MSC, The Woodlands, **2000**

[18] a) F. C. Grozema, L. D. A. Siebbeles, J. M. Warman, S. Seki, S. Tagawa, U. Scherf, *Adv. Mater.* **2002**, *14*, 228–231; b) A. Acharya, S. Seki, A. Saeki, Y. Koizumi, S. Tagawa, *Chem. Phys. Lett.* **2005**, *404*, 356–360; c) A. Saeki, S. Seki, T. Sunagawa, K. Ushida, S. Tagawa, *Philos. Mag.* **2006**, *86*, 1261–1276; d) K. Nagashima, T. Yanagida, H. Tanaka, S. Seki, A. Saeki, S. Tagawa, T. Kawai, *J. Am. Chem. Soc.* **2008**, *130*, 5378–5382.

[19] a) S. Seki, Y. Yoshida, S. Tagawa, K. Asai, K. Ishigure, K. Furukawa, M. Fujiki, N. Matsumoto, *Philos. Mag. B* **1999**, *79*, 1631–1645; b) H. Imahori, M. Ueda, S. Kang, H. Hayashi, S. Hayashi, H. Kaji, S. Seki, A. Saeki, S. Tagawa, T. Umeyama, Y. Matano, K. Yoshida, S. Isoda, M. Shiro, N. V. Tkachenko, H. Lemmetyinen, *Chem. Eur. J.* **2007**, *13*, 10182–10193; c) I. Hisaki, Y. Sakamoto, H. Shigemitsu, N. Tohnai, M. Miyata, S. Seki, A. Saeki, S. Tagawa, *Chem. Eur. J.* **2008**, *14*, 4178–4187; d) T. Amaya, S. Seki, T. Moriuchi, K. Nakamoto, T. Nakata, H. Sakane, A. Saeki, S. Tagawa, T. Hirao, *J. Am. Chem. Soc.* **2009**, *131*, 408–409.

Received: July 1, 2010
Published online: September 6, 2010

